

with
corrections

DISLOCATION MODEL FOR ASEISMIC FAULT SLIP IN THE TRANSVERSE RANGES
OF SOUTHERN CALIFORNIA

ABE CHENG⁽¹⁾, DAVID D. JACKSON⁽¹⁾, AND MITSUHIRO MATSU'URA⁽²⁾

(1) Department of Earth & Space Sciences, UCLA, Los Angeles, California,
USA

(2) Geophysical Institute, Faculty of Science, University of Tokyo,
Bunkyo-ku, Tokyo 113, Japan



ABSTRACT

Geodetic data at a plate boundary can reveal the pattern of subsurface displacements that accompany plate motion. We model these displacements as the sum of rigid block motion and the elastic effects of frictional interaction between blocks. We represent the frictional interactions by uniform dislocation on each of several rectangular fault patches. We then estimate the block velocities and fault parameters from geodetic data. Our Bayesian inversion procedure employs prior estimates based on geological and seismological data. We apply the method to the Transverse Ranges, using prior data from Bird and Rosenstock (1984) and geodetic data from the USGS trilateration networks. Our model consists of 11 blocks and 26 rectangular fault patches. The block motion inferred from the geodetic data has the same order of magnitude as the

geologic estimates, and for many faults the agreement is excellent. However, the geodetic data imply a displacement rate of about 20 mm/yr across the San Andreas Fault, while the geologic estimates exceed 30 mm/yr. The prior model and the final estimates both imply about 10 mm/yr crustal shortening normal to the trend of the San Andreas Fault. Most of this shortening occurs on the Sierra Madre-Cucamonga and the White Wolf Fault systems. Aseismic fault motion is a major contributor to plate motion, and the thickness of the frictional surface varies considerably from one fault to another. The geodetic data can help to identify faults that are suffering rapid stress accumulation; in the Transverse Ranges those faults are the San Andreas and the Santa Susana.

**ORIGINAL PAGE IS
OF POOR QUALITY**

INTRODUCTION

Since 1971 the U.S. Geological Survey (USGS) have carried out precise length measurements on baselines near the San Andreas Fault system in California (Savage et al., 1981). These measurements tell us much about the details of plate motion, and the process of stress accumulation leading to earthquakes.

In this paper we address the following questions: (1) How wide is the plate boundary, and can the plate motion be blamed on specific known faults? (2) Do the geodetic data agree with conclusions based on geologic observations and plate tectonic models? (3) Which faults are accumulating stress most rapidly?

King and Savage (1984) analysed trilateration data for the Transverse Ranges using a simple dislocation model. They showed that the strain rate is relatively low in this region, compared to other locations along the San Andreas Fault. This implies that the displacement rate on the San Andreas at depth is lower here than elsewhere, or that the San Andreas is locked to a great depth here, or possibly that displacement is taking place on faults outside of the trilateration network. They found that there were significant spatial variations in strain rate, and that the data could be fit reasonably well by a model with only two faults: the San Andreas and the Garlock. Their preferred model had 20 mm/yr of right lateral slip on the San Andreas, and 8 mm/yr left lateral slip on the Garlock, with both faults locked to a depth of 15 km.

4

We are able to include many more faults than previous investigators because we use a new nonlinear inversion procedure incorporating prior estimates of all the parameters. The prior estimates are based on geologic and seismological data. By including many more faults, we get a much more realistic model of the plate boundary region, and we can test the importance of many previously neglected faults.

Our dislocation model is described more thoroughly in a separate paper (Matsu'ura et al., 1986) reporting a similar analysis of the Hollister area of central California. The inversion method is described in detail in Jackson and Matsu'ura (1985).

DISLOCATION MODEL

Assumptions

We assume that geodetic displacements, and the block and fault motions that cause them, are constant in time over the period 1971-1983. Thus we use rates of change of line length as our basic data, and velocities and displacement rates as our primary unknown parameters. By using geological estimates of block velocities in our prior model, we implicitly assume that displacement rates are constant over periods of many thousand years. The latter assumption is a working hypothesis, which we can test. If the final model agrees with the geological estimates, then the hypothesis of constant displacement rate cannot be rejected by our data. If in addition the parameters are well resolved by the geodetic data, then the final estimate is relatively independent of the prior model; in that case agreement between the prior and final estimates tends to confirm the constant rate hypothesis.

We represent the crust by an elastic half-space divided into a finite number of blocks. The fault surfaces separating these blocks are divided somewhat arbitrarily into segments from 10 to 100 km long. In the absence of friction, the blocks would slide freely with no shear stress accumulation. However, friction on the upper part of the fault surface restricts motion and causes stress. We divide each fault segment into an upper "brittle zone" and a lower "ductile zone". The depth of the boundary between these zones is called the

"locking depth;" the width of the brittle zone, measured in the fault plane, is called the "fault width." For vertical faults the locking depth and fault width are identical. In the ductile zone, the displacement rate across the fault is simply the velocity difference of the two blocks separated by the fault. In the brittle zone, the net displacement rate is the difference between the relative block velocity and the dislocation rate. This dislocation rate is introduced to represent the effects of frictional interaction, and it is assumed to be constant over each dislocation patch. The dislocation rate is essentially a displacement deficit, likely to be repaid in the form of earthquakes or other episodic displacements at a later date. A schematic view of a single fault segment, and the notation we use to describe it, are shown in Fig. 1.

If the entire surface separating two blocks were sliding freely, there would be no dislocation motion nor stress accumulation, and the surface displacement would be rigid block motion only. If the upper fault patch were completely locked, then the dislocation motion would equal the block motion, and stress would accumulate at a rate depending on the locking depth and the relative block velocity.

We use the Jennings et al. (1975) fault map of California to determine block boundaries and the location of the upper corners of each fault segment. These are held fixed in our analysis. The width and dip angle of each fault patch, and the dislocation rate vector, are estimated from the trilateration data. The block boundaries

that we assume are shown in Fig. 2, along with the actual traces of faults.

Over geologic time, the fitful motion in the brittle zone of any fault segment should average to the same rate as that of the lower ductile zone. Thus, the loading of the upper fault zone by frictional stress and its unloading by earthquakes are each temporary aberrations; the geological displacement rates should be compared to the steady "block motion" in our geodetic model. In the short term, friction at the upper part of the fault surface will cause some temporary distortion of the block: it is this distortion that we model with the dislocation. In order to distinguish the effects of block motion from the distortion near the block boundaries, we need to observe displacement both close to and far from the boundary. For many faults in the study area this condition is satisfied, and we can resolve well the dislocation motion that causes stress to build up on the fault.

Calculating the rate of line length change caused by block motion is simple; the velocity of each monument is just the velocity of the block on which it rides. The rate of line length change between any two monuments is the projection of the velocity difference between the two sites onto the position vector from one site to the other. For the dislocations, we compute theoretical displacements and partial derivatives with respect to parameter values using the method of Matsu'ura (1977), summarized briefly in Matsu'ura et al. (1986). We assume that the earth is a uniform elastic half-space, with the Lamé constants equal.

Primary Parameters

The primary parameters consist of the eastward and northward velocity components for each block; and the dislocation rate (\dot{D}), fault width (W), dip angle (δ), and slip angle (λ) for each fault patch. In the Transverse Ranges we assume 11 blocks and 26 fault segments, so we have 22 block parameters and 104 fault parameters, for a total of 126. The dip angle is defined such that 90 degrees is vertical. The slip angle is defined so that if the dislocation rate is positive, then 0 degrees represents left lateral strike slip motion, 90 degrees represents pure dip slip motion, and 180 degrees represents right lateral strike slip. If the dislocation rate is negative, then 0 and 180 degrees represent right and left lateral displacement deficits, respectively.

Derived Parameters

We also compute estimates of several derived parameters that are functions of the primary parameters. The "block slip" is the tangential component (parallel to the block boundary) of the relative velocity between two blocks. It depends on the block velocities and the orientation of the boundary. Positive block slip denotes right lateral motion. The "block convergence" is the component of relative motion normal to the boundary, measured such that convergence is positive. "Strike slip" and "dip slip" are the horizontal and updip components of the dislocation motion. A positive strike slip value indicates a right lateral displacement

deficit, and a positive dip slip value indicates a convergence deficit. "Creep rate" is the difference between the block slip and the strike slip. In other words, block slip is the tangential displacement rate at depth (below the dislocation patch), and creep rate is the shallow slip rate.

Of course the earth is not a homogeneous halfspace, and fault displacement rates probably do not change discontinuously at rectangular patch boundaries. The fault dislocation parameters represent averages over the fault zone, rather than specific values appropriate for any specific location. Similarly the "creep rate" represents the average shallow displacement inferred from geodetic baselines a few km long, and it might not be the same quantity that is observed with short baseline creepmeters across some faults.

For very long strike slip faults, the rate of stress accumulation can be calculated from the dislocation parameters; roughly, it is directly proportional to the dislocation rate and inversely proportional to the fault width. Assuming some fixed value for stress drop in a large earthquake, one can then calculate the recurrence time and the characteristic displacement for such earthquakes. We give the relevant equations and calculate some estimated values of these parameters for faults in the Hollister Region in Matsu'ura et al. (1986). We do not report such calculations for the Transverse Ranges, because the required assumptions are questionable in this region complicated by many fault intersections and dip-slip faults.

INVERSION METHOD

In our analysis the data are observed rates of change of line length, while the model parameters are the east and north components of each block velocity; and the dislocation rate, fault width, dip angle, and slip angle of each fault patch. The observed length rates are essentially linear functions of the block velocities and dislocation rates, but they are nonlinear functions of fault width, dip angle, and slip angle. Because of the large number of potentially active faults, the data may be insufficient to resolve all of the relevant unknown parameters. Thus we are faced with a nonlinear, possibly underdetermined inverse problem. However, we know a fair amount about the expected values of the parameters, independent of the geodetic data. For example, the block velocities should be the same order of magnitude as the geologically observed rates, and the dip and slip angle should agree with geological observations. Assuming that earthquakes occur in the brittle zone we can estimate the fault width at least approximately. It is then appropriate to use a nonlinear Bayesian procedure that makes use of the relevant prior information. We use a method described in detail by Jackson and Matsu'ura (1985), and summarized only briefly here. Suppose that we have n observation equations and m unknown parameters, and let

$$\underline{e} = \underline{y} - \underline{f}(\underline{x})$$

where \underline{y} is an n-vector of observed data, \underline{x} is an m-vector of unknown parameters, \underline{f} is a vector of possibly nonlinear functions

giving the predicted values corresponding to the observations, and \underline{e} is an n -vector of residuals. The equation above is referred to as the "observation equations." Suppose also that we have prior estimates \underline{x}_0 for each of the parameters, and let

$$\underline{d} = \underline{x}_0 - \underline{x}$$

be an m -vector of residuals to the prior estimates. If the errors in the observations and prior estimates can be described as random variables with mean equal to zero and covariance matrices \underline{E} and \underline{D} , respectively, then the minimum variance estimate of \underline{x} minimizes

$$T^2 = \underline{e}^T \underline{E}^{-1} \underline{e} + \underline{d}^T \underline{D}^{-1} \underline{d}$$

Minimizing T^2 is equivalent to minimizing the sum of squared residuals to the combined set of equations

$$\underline{e}' = \underline{F}\underline{y} - \underline{F}\underline{f}(\underline{x})$$

$$\underline{d}' = \underline{G}\underline{x}_0 - \underline{G}\underline{x}$$

where $\underline{F}^T \underline{E} \underline{F} = \underline{I}$ and $\underline{G}^T \underline{D} \underline{G} = \underline{I}$. The matrices \underline{F} and \underline{G} serve to standardize the observed and prior data, so that the equations above may be combined and solved by a standard nonlinear least squares estimation package. The prior estimates stabilize the inversion, but there is no need to treat them differently from the observation equations in computation.

Assuming that the functions $f(\underline{x})$ are linear within a large enough neighborhood of the solution, the probable estimation errors are described by the asymptotic covariance matrix

$$\underline{X} = (\underline{A}^T \underline{E}^{-1} \underline{A} + \underline{D}^{-1})^{-1}$$

and the resolution matrix (Jackson and Matsu'ura, 1985) is

$$\begin{aligned} \underline{R} &= \underline{X} \underline{A}^T \underline{E}^{-1} \underline{A} \\ &= \underline{I} - \underline{X} \underline{D}^{-1} \end{aligned}$$

\underline{R} is an m by m matrix, whose diagonal elements give for each parameter the relative sensitivity of the final result to the observations. The complement (one minus the diagonal element) gives the relative sensitivity to the prior estimates. In the tables of parameter estimates below, the "resolution" for each parameter is the corresponding diagonal element of the resolution matrix, multiplied by 100 to convert to %.

The reported error estimates for each parameter are the standard errors, or square roots of the relevant diagonal elements of the modified covariance matrix \underline{X}' , defined as

$$\underline{X}' = v^2 \underline{X}.$$

where $v^2 = T^2/n$. v^2 is the "variance inflation factor," whose purpose is to adjust the uncertainties to match the observed sum of squared residuals. We did not modify the covariances \underline{C} and \underline{D} , so that the

final error estimates for some parameters are larger than the prior uncertainties.

DATA

14
ORIGINAL PAGE IS
OF POOR QUALITY

Trilateration data

We use line length data provided by Dr. James Savage and his group at USGS in Menlo Park, California. For each line, we determined the rate of change of line length and its standard error by linear regression of length on time. The standard error is adjusted to be consistent with the length residuals, so that if the line length is quite linear with time, then the standard error will be small. In general, the standard error will decrease in proportion to the time span covered by the measurements. We assume that data errors are uncorrelated, so that the data covariance matrix C is a diagonal matrix whose diagonal elements are the squares of the corresponding standard errors. We use data for 160 lines from the USGS Palmdale, Tehachapi, San Gabriel, Los Padres, and San Fernando networks. The locations of the monuments are shown in Fig. 2. The length change rates and their standard errors are tabulated in Cheng (1985) and will be furnished on request.

Prior estimates

We take prior estimates of block velocities from the model of Bird and Rosenstock (1984). Their model was adjusted to fit geologically observed displacement rates on major faults in southern California and the plate motion estimates of Minster and Jordan (1978). We make a few minor adjustments to their model: we modify some block boundaries slightly, and we combine their Santa Barbara

Channel, Chino, San Pedro, Santa Anna, and Vallecito blocks into a single block because they found negligible displacement between them. We assume rather generous prior uncertainties (20 mm/yr in each component) to allow for temporal changes from the geological average displacement rates. The prior estimates and their uncertainties appear in Table 1, along with our final estimates, which are discussed below.

We assume prior estimates of the fault dislocation rate to offset the block displacements at the surface, except for a few faults such as "San Andreas F" where creep is observed. There, we choose a smaller dislocation rate, so that the difference between block slip and strike slip dislocation movement would equal the observed creep rate. We assume generous prior uncertainties for the dislocation rate as well; 20 mm/yr for most faults, and 10 mm/yr for a few less active faults. We assume that the fault width is 10 ± 5 km for all faults, based on the observation that most earthquakes, assumed to occur in the brittle zone, have depths in this range. For strike slip faults we assume to have a dip of 90 ± 10 degrees, except for the Santa Ynez and Pine Mtn faults which we give an uncertainty of 30 degrees. For thrust faults we assume a dip of 65 ± 20 degrees. The Big Pine, San Cayetano, Sta Susana, San Gabriel, Sierra Madre, and Cucumonga are assumed to dip down to the north, while the White Wolf and Pleito dip down to the south in our prior model. Prior estimates of slip angle are 180 degrees for strike slip faults, and 90 degrees for dip slip faults, with uncertainties ranging from 10 to 30 degrees depending on the geological complexity of the area. Table 2 shows the prior estimates and uncertainties of

14

all fault parameters, and Table 3 shows the derived parameters corresponding to the prior estimates.

RESULTS

Goodness of fit

The block and fault model fits the trilateration data reasonably well, although the final rms residual is about 1.4 times the estimated standard deviation of the data. This modest discrepancy might be caused by nontectonic deformation at some sites, by motion of neglected faults, by systematic errors in the data, or even by bad luck (that is, random coincidence). The presence of a few large residuals (two with absolute residual exceeding four standard deviations) suggests that there are some problems with a few of the data, especially from lines involving stations Tenhi, Pe2, and Tuj rml. Nevertheless the fit is good enough that there is no cause to doubt the overall data quality, or the estimated standard deviations of the data.

Block velocities and missing slip on the San Andreas

Block velocities are shown in Table 1 and Fig. 3. The block velocities are resolved into parallel (block slip) and perpendicular (block convergence) components for each block boundary in Table 3. Fig. 4 shows the block slip, and Fig. 5 the block convergence. Referring to Table 1, we see that except for the Mojave block, which is fixed as a reference by a very strongly constrained prior estimate, the block velocities are resolved very well. They differ substantially from the prior estimates, in sharp contrast with our results for Hollister (Matsu'ura et al., 1986), where the

estimated block velocities agree remarkably well with the geological estimates. In the Hollister region, our geodetic analysis showed 36 mm/yr of relative motion for blocks within the array; this compares with 34 mm/yr estimated from geological fault displacements, and leaves about 20 mm/yr to occur outside the network, presumably to the west, if the total motion is to match the plate tectonic estimates of 56 mm/yr (Minster and Jordan, 1978). In the Transverse Ranges, the geodetic data account for only about 20 mm/yr of net motion across the geodetic array (that is, between the Malibu block (F) and the Mojave block (K). Following Bird and Rosenstock (1984) we assume that the Mojave block travels about 14 mm/yr in the direction N11W with respect to the stable North American continent; then the Malibu block is moving 33 mm/yr at N29W with respect to North America. Thus, the geodetic data fall about 25 mm/yr short of matching the predicted plate motion in the Transverse Ranges, compared to 20 mm/yr at Hollister. However at Hollister, the geodetic data match the geological observations, while in the Transverse ranges they don't.

At Hollister, much of the shortfall between geodesy and plate tectonics is easily explained by additional displacements west of the network. In fact Hall (1981) and others estimate that 10 to 15 mm/yr right lateral displacement may have occurred on the San Simeon-Hosgri fault during the last 3 Myr. In the Transverse Ranges, a similar amount of displacement could be blamed on offshore faults, but there is still a direct conflict between the geodetic and geological estimates of motion on the San Andreas Fault system. Our prior model, based on the geological compilation of Bird and

Rosenstock^A, has the Malibu block moving almost 47 mm/yr at N52W with respect to the Mojave block. Our final model gives 20 mm/yr at N40W. (1984)

Possible explanations for the discrepancy between geodesy and geology in the Transverse Ranges are (a) the geodetic and geologic rates are not comparable because of temporal variations in displacement rate, (b) the geodetic estimates are in error, or (c) the geologic estimates err.

We do not believe that time dependent block motion, hypothesis (a) above, provides the answer. While the near surface fault motions vary with time, the deeper block motions appear to be quite steady. This assertion is based on the close agreement between geodesy and plate tectonics in the Salton Trough (Savage et al., 1979; Cheng, 1985), and on the close agreement between geodesy and geology for Hollister (Matsu'ura et al., 1986). But of course this evidence is circumstantial, and our assumption of constant block velocities over many thousands of years may fail.

Errors in the geodetic model (hypothesis b) could result from erroneous data, or from a mistake in modeling. Data errors are very unlikely to be a serious problem in this analysis. While some systematic errors may cause annual or other short period variations (Jackson et al., 1983), such errors would have very little effect on the secular rates of line length change (Cheng, 1985). The trilateration data for the Transverse Ranges and for Hollister were collected by identical methods, and no discrepancy occurs at

20

Hollister. A possible modeling error could result from our assigning a prior fault width of 10 ± 5 km. The estimated fault width is poorly resolved (see discussion below), so that the final fault width estimate is strongly influenced by the prior. If the San Andreas Fault were locked to a much greater depth, then some of the resulting strain would occur outside of the network, and greater block motion would be required to match the observed displacements. We performed some calculations assuming much greater fault width on the San Andreas, and we found that the estimated block slip could match the geological observations if the fault is locked to 25 km or more (about the thickness of the crust). This seems much too deep to us, because earthquakes on this section of the San Andreas rarely exceed 15 km depth (Webb and Kanamori, 1985), and because the estimated fault width rarely exceeds 15 km in areas where it is well resolved (Cheng, 1985; Matsu'ura et al., 1986). Nevertheless, we cannot completely reject the idea that the San Andreas is presently locked to the base of the crust within the Transverse Ranges.

Errors in the geologic rates of Bird and Rosenstock⁽¹⁹⁸⁴⁾ are not unthinkable. They constrained their model to agree with plate tectonics, possibly causing them to blame the San Andreas for motion that actually occurred on unknown faults. The Bird and Rosenstock model is supported by good independent data for fault "San Andreas A," north of the big bend (Clark et al., 1985; Dickinson et al., 1972; Sieh and Jahns, 1984), where 30 mm/yr seems to be the minimum believable slip rate. However, on sections B-E, there is little data, and that published only in abstract form (Rust, 1982). Data for the southern section (F) suggest that 30 mm/yr is an upper

limit. Humphries and Weldon (1984) suggest a much lower rate for the San Andreas, more consistent with our final estimates. The last word is yet to be written on this question, and it is conceivable that after further investigation the geological estimates will come into agreement with the geodetic values.

In summary, we cannot rule out any of the listed hypotheses to explain the discrepancy between our estimated block velocities and the geological prior model. It could be that the two are not comparable because block rates vary, or that we have badly underestimated the locking depth of the San Andreas, or that the geological estimates are off by 10-20 mm/yr.

Convergence across the Transverse Ranges

Our results confirm the assertion of Bird and Rosenstock (1984) that substantial shortening occurs across the Transverse Ranges. Table 3 and Fig. 5 show about 10 mm/yr of block convergence across the Sierra Madre-Cucamonga Fault system, with comparable values for the Northern San Andreas, Pleito, and White Wolf Faults. The estimated convergence is statistically significant at the 95 % confidence level for the San Gabriel W, Sierra Madre, Cucamonga, and Pleito Faults. For statistical significance, we use the approximate criterion that the absolute value of the parameter estimate should exceed twice the standard error. We did not calculate resolution estimates of derived parameters, but it is clear that the estimates of block convergence come almost entirely from the trilateration data because the block convergence is derived from the well resolved

block velocities, and because the final uncertainty is much smaller than the prior uncertainty.

Humphries and Weldon (1984) objected to the convergence implied by Bird and Rosenstock⁽¹⁹⁸⁴⁾ because such convergence should cause massive crustal accumulation where only modest thickening is observed. It is not impossible that the convergence in our model results from systematic error causing an apparent secular decrease in line length. However, possible systematic errors have been quite exhaustively studied (Savage and Prescott, 1983; Jackson *et al.*, 1983; Savage and Gu, 1985) and none has been identified that would cause a spurious secular dilatation. Another possible explanation is that end effects from fault motion outside the array (on the central San Andreas, for example) would cause local contraction. However, this explanation is inadequate to explain the observed widespread convergence. We believe our estimates indicate true tectonic convergence, and that some explanation must be found for the missing crust.

Dislocation rates

The dislocation rates, listed in Table 2, are generally well resolved, but only for a few faults (are they) statistically significant at the 95% confidence level. The dislocation rates are projected into their strike slip and dip slip components in Table 3. The faults with significant strike slip dislocation rates are the Santa Susana E., and the San Andreas A-E. None of the geodetic monuments in our study were close to the

southernmost section of the San Andreas (section F) so the dislocation rate there is uncertain and poorly resolved. Dip slip fault displacement is statistically significant at the 95 % confidence level for only four faults: Santa Susana E, San Gabriel W, Cucamonga, and Pleito (Table 3). The larger values (for the latter three faults) are not geophysically reasonable, and we do not suggest that they be taken seriously. These erroneously high rates serve to adjust the motion of monuments very close to the faults from those predicted by the block motion. Because of the steep dip on the faults, the large dip slip displacements have a relatively small effect on the horizontal component of motion, which is what is actually measured. In specifying prior information, we did not adequately constraint the dislocation motion for dip slip faults. The erroneous dip slip motion will have little effect on other parameters for the San Gabriel W and Cucamonga, because of their very shallow depth. However, the Pleito is deeper, and the unreasonable estimate of the dip slip motion could cause a moderate error in the block motion for the Pleito Hills block.

Fault width

The fault width, listed in Table 2, is generally poorly resolved and seldom differs from the prior estimate by more than twice the standard error. Only for the San Gabriel W and the Sierra Madre Fault does the resolution exceed 80 %; both are dip slip faults with very small estimated widths. For two reasons we do not believe these fault widths are reliable, even if the asymptotic variance is small. First, we have found that the calculated length

rates are strongly nonlinear functions of the fault width for shallow faults. Second, we have not provided adequate prior information for dip slip faults, so that the near-surface dip slip fault motion is poorly constrained in our model. This problem may also affect the depth estimates for shallow dip slip faults.

In the Hollister area, Matsu'ura et al. (1986) find resolvable depth variations on strike slip faults without the ambiguities present in the Transverse Ranges. Estimated fault widths varied from a few km to 14 km. As mentioned above, a fault width of 25 km or more on the San Andreas would help to reconcile geodetic and geologic slip estimates, although the geodetic data cannot resolve this fault width. Nevertheless, the Hollister analysis shows that locking depth varies considerably from place to place, and the data for the Transverse Ranges add mild support. Local variations in earthquake depths (for example, Webb and Kanamori, 1985) add further support.

CONCLUSIONS

Estimated block velocities are well resolved. They show statistically significant strike slip at depth on the San Gabriel N, all segments of the San Andreas, the White Wolf E, and the Garlock E. Cumulative strike slip motion is revealed in the relative block velocity between the Malibu and Mojave blocks, which amounts to only 20 mm/yr in the direction N40W. This estimate is approximately half of the geologically determined rate on the San Andreas. The apparent shortfall of geodetic slip could be explained by temporal variability of slip at depth, locking of the San Andreas to 25 km or more, or errors in the geological estimates. In any case there is geodetically observable slip on diverse faults, and the plate boundary region must be considerably wider than the geodetic network, about 75 km in extent. The geodetic data show unambiguous crustal shortening in excess of 10 mm/yr normal to the San Andreas system, mostly on the Sierra Madre-Cucamonga and White Wolf Faults.

ACKNOWLEDGEMENTS

We thank the U.S. National Aeronautics and Space Administration who provided support via grant NAG 5447. We thank Dr. James Savage, Dr. Will Prescott, and Dr. Nancy King for generously supplying the data and explaining details of its collection and reduction. Prof. Peter Bird provided many valuable suggestions during the course of this project.

REFERENCES

Dickinson, W.R., Cowan, D.S., and Schweikert, R.A., 1972. Test of new global tectonics: discussion. American Association of Petroleum Geologists Bulletin, 56: 375-384.

Bird, P., and Rosenstock, R.W., 1984. Kinematics of present crust and upper mantle flow in southern California. Geol. Soc. Amer. Bull., 95: 946-957.

Cheng, A., 1985. Deformation of the San Andreas Fault systems inferred from trilateration measurements. Ph.D. Thesis, Department of Earth and Space Sciences, University of California at Los Angeles, 373 pp.

Clark, M.N., Lienkaemper, J.J., Harwood, D.S., Lajoie, K.R., Matti, J.C., Perkins, J.A., Rymer, M.J., Sarna-Wojcicki, A.M., Sharp, R.V., Sims, J.D., Tinsley, J.C., and Ziony, J.I., 1985. Preliminary slip rate table for Quaternary faults of California. U. S. Geological Survey Open File Report.

Hall, C.A., 1981. San Luis Obispo transform fault and middle Miocene rotation of the western Transverse Ranges, California. J. Geophys. Res., 86: 1015-1031.

Humphries, E.D., and Weldon, R., 1984. A kinematic model of southern California (Abstract). EOS (Amer. Geophys. Union

Transactions), 65: 992.

Jackson, D.D., and Matsu'ura, M., 1985. A Bayesian approach to nonlinear inversion. J. Geophys. Res., 90: 581-591.

Jackson, D.D., Cheng, A., and Liu, C.C., 1983. Tectonic motions and systematic errors in leveling and trilateration data for California. Tectonophysics, 97: 73-83.

Jennings, C.W., Strand, R.G., Rogers, T.H., Stinson, M.G., Burnett, J.L., Kahle, J.E., Streitz, R., and Switzer, R.A., 1975. Fault map of California with locations of volcanoes, thermal springs, and thermal well, 1:750,000. California Division of Mines and geology Geologic Map no. 1.

King, N.E., and Savage, J.C., 1984. Regional Deformation near Palmdale, California, 1973-1983. J. Geophys. Res., 89: 2471-2477.

Matsu'ura, M., 1977. Inversion of geodetic data. I: Mathematical formulation. J. Phys. Earth, 25: 69-90.

Matsu'ura, M., Jackson, D.D., and Cheng, A., 1986. Dislocation model for aseismic fault motion at Hollister, California. J. Geophys., Res., submitted.

Minster, J.B., and Jordan, T.H., 1978. Present-day plate motions. J. Geophys. Res., 83: 5331-5334.

Rust, D.J., 1982. Evidence for uniformity of large earthquakes in the "big bend" of the San Andreas Fault. ^(Abstract) EOS (Amer. Geophys Union Trans.), 63: 1030.

Savage, J.C., and Gu Guohua, 1985. The 1979 Palmdale, California ^{if} strain event in retrospect. J. Geophys. Res., 90: 10301-10309.

Savage, J.C., and Prescott, W.H., 1983. The precision of geodolite surveys: a reply to Jackson and Cheng. J. Geophys. Res., 88: 10478-10484.

Savage, J.C., Prescott, W.H., Lisowski, M., and King, N.E., 1979. Deformation across the Salton Trough, California, 1973-1977. J. Geophys. Res., 84: 3069-3079.

Savage, J.C., Prescott, W.H., Lisowski, M., and King, N.E., 1981. Strain accumulation in southern California, 1973-1980. J. Geophys. Res., 86: 6991-7001.

Sieh, K.E., and Jahns, R.H., 1984. Holocene activity of the San Andreas fault at Wallace Creek, California. Geol. Soc. Amer. Bull., 95: 883-896.

Thatcher, W., 1975. Strain accumulation on the northern San Andreas fault zone since 1906. J. Geophys. Res., 80: 4873-4880.

Webb, T.H., and Kanamori, H., 1985. Earthquake focal mechanisms in the eastern Transverse Ranges and San Emigdio Mountains, southern

California, and evidence for a regional decollement. Bull. Seis. Soc. Amer., 75: 737-758.

Table 1

Block Parameters

Block/ model	East (mm/yr)	Res (%)	North (mm/yr)	Res (%)	Magnitude (mm/yr)	Direction (deg)
A Cuyama						
prior	-25.1 ±	20.0	26.9 ±	20.0	36.8	-43
final	-20.5 ±	4.2 98	23.9 ±	3.6 98	31.5	-41
B Big Pine Mtn						
prior	-26.4 ±	20.0	29.3 ±	20.0	39.4	-42
final	-22.9 ±	3.3 99	24.1 ±	3.5 98	33.2	-44
C Cachuma						
prior	-32.5 ±	20.0	31.4 ±	20.0	45.2	-46
final	-18.3 ±	4.0 98	25.3 ±	3.1 99	31.2	-36
D Frazier						
prior	-32.5 ±	20.0	31.4 ±	20.0	45.2	-46
final	-24.9 ±	4.6 97	25.2 ±	3.1 99	35.4	-45
E Piru						
prior	-32.5 ±	20.0	31.4 ±	20.0	45.2	-46
final	-15.9 ±	2.8 99	26.7 ±	2.1 99	31	-31
F Malibu						
prior	-39.4 ±	20.0	42.3 ±	20.0	57.8	-43
final	-15.9 ±	2.4 99	29.1 ±	2.0 99	33.2	-29
G San Gabriels						
prior	-36.7 ±	20.0	27.7 ±	20.0	46	-53
final	-17.5 ±	2.6 99	19.7 ±	1.2 100	26.4	-42
H San Joaquin						
prior	-3.6 ±	20.0	4.6 ±	20.0	5.8	-38
final	-13.8 ±	5.2 96	0.5 ±	6.8 94	13.9	-88
I Pleito Hills						
prior	-0.7 ±	20.0	20.1 ±	20.0	20.1	-2
final	-1.9 ±	5.2 96	20.2 ±	3.4 98	20.3	-5
J Tehachapi						
prior	-5.0 ±	20.0	17.3 ±	20.0	18	-16
final	-7.2 ±	2.5 99	11.6 ±	1.3 100	13.7	-32
K Mojave						
prior	-2.6 ±	.0	13.5 ±	.0	13.7	-11
final	-2.6 ±	.0 0	13.5 ±	.0 0	13.7	-11

Table 2.

Primary Fault Parameters

Fault/ model	\dot{D} (mm/yr)	Res (%)	W (km)	Res (%)	δ (deg)	Res (%)	λ (deg)	Res (%)
1 Ozena								
prior	3.0 ± 20.0		10 ± 5		90 ± 10		180 ± 10	
final	3.0 ± 7.1	93	10 ± 7	2	90 ± 14	0	182 ± 13	1
2 Big Pine W								
prior	6.0 ± 20.0		10 ± 5		90 ± 10		180 ± 10	
final	-6.2 ± 5.2	96	9 ± 7	4	93 ± 13	2	181 ± 13	3
3 Big Pine C								
prior	6.0 ± 20.0		10 ± 5		90 ± 30		180 ± 30	
final	2.1 ± 9.6	87	10 ± 7	0	89 ± 40	1	180 ± 41	0
4 Big Pine E								
prior	9.0 ± 20.0		10 ± 5		115 ± 20		180 ± 20	
final	5.0 ± 7.7	92	10 ± 7	2	115 ± 27	3	181 ± 27	1
5 Pine Mtn W								
prior	.0 ± 10.0		10 ± 5		90 ± 30		180 ± 30	
final	-8.4 ± 6.7	76	11 ± 6	16	118 ± 34	28	167 ± 38	14
6 Sta Ynez W								
prior	.0 ± 10.0		10 ± 5		90 ± 30		180 ± 30	
final	3.7 ± 10.5	40	10 ± 7	0	93 ± 40	1	176 ± 40	4
7 Sta Ynez E								
prior	.0 ± 10.0		10 ± 5		90 ± 30		180 ± 30	
final	-4.4 ± 5.6	83	10 ± 7	1	85 ± 39	7	169 ± 38	11
8 Pine Mtn E								
prior	.0 ± 10.0		10 ± 5		90 ± 30		180 ± 30	
final	-1.9 ± 10.9	37	10 ± 7	0	91 ± 41	0	178 ± 41	1
9 San Cayetano								
prior	.0 ± 20.0		10 ± 5		115 ± 20		90 ± 20	
final	-11.4 ± 8.6	90	11 ± 6	11	91 ± 15	71	112 ± 16	64
10 Sta Susana W								
prior	.0 ± 20.0		10 ± 5		115 ± 20		90 ± 20	
final	3.1 ± 4.9	97	12 ± 7	3	118 ± 20	43	80 ± 23	25
11 Sta Susana E								
prior	.0 ± 20.0		10 ± 5		115 ± 20		90 ± 20	
final	8.0 ± 2.5	99	10 ± 3	74	38 ± 12	79	31 ± 10	87
12 San Gabriel N								
prior	.0 ± 20.0		10 ± 5		115 ± 20		90 ± 20	
final	17.7 ± 12.2	80	12 ± 6	26	138 ± 14	74	114 ± 22	33
13 San Gabriel W								
prior	.0 ± 20.0		10 ± 5		115 ± 20		90 ± 20	
final	-40.0 ± 10.0	87	3 ± 1	97	117 ± 9	88	64 ± 11	82

Table 2.

Primary Fault Parameters

Fault/ model	D (mm/yr)	Res (%)	W (km)	Res (%)	δ (deg)	Res (%)	λ (deg)	Res (%)
14 Sierra Madre								
prior	.0 ± 20.0		10 ± 5		115 ± 20		90 ± 20	
final	-30.8 ± 17.7	57	3 ± 2	87	120 ± 11	84	82 ± 15	70
15 Cucamonga								
prior	.0 ± 20.0		10 ± 5		115 ± 20		90 ± 20	
final	-21.9 ± 8.7	90	7 ± 6	22	114 ± 21	38	110 ± 18	58
16 San Andreas A								
prior	.0 ± 20.0		10 ± 5		90 ± 10		180 ± 10	
final	-21.9 ± 8.7	90	13 ± 6	27	90 ± 13	12	179 ± 12	18
17 San Andreas B								
prior	31.0 ± 20.0		10 ± 5		90 ± 10		180 ± 10	
final	23.8 ± 5.4	96	13 ± 6	27	92 ± 13	8	181 ± 13	4
18 San Andreas C								
prior	35.0 ± 20.0		10 ± 5		90 ± 10		180 ± 10	
final	17.7 ± 8.3	91	10 ± 6	21	92 ± 13	8	181 ± 13	4
19 San Andreas D								
prior	35.0 ± 20.0		10 ± 5		90 ± 10		180 ± 10	
final	34.3 ± 14.2	73	12 ± 6	8	96 ± 13	10	183 ± 11	33
20 San Andreas E								
prior	35.0 ± 20.0		10 ± 5		90 ± 10		180 ± 10	
final	13.0 ± 4.1	98	12 ± 6	30	94 ± 12	15	174 ± 11	39
21 San Andreas F								
prior	35.0 ± 20.0		10 ± 5		90 ± 10		180 ± 10	
final	16.6 ± 2.8	99	12 ± 3	79	106 ± 7	73	171 ± 6	83
22 White Wolf W								
prior	.0 ± 20.0		10 ± 5		90 ± 10		180 ± 10	
final	-25.6 ± 22.3	32	12 ± 7	6	89 ± 14	0	179 ± 14	0
23 White Wolf E								
prior	-0.2 ± 20.0		10 ± 5		65 ± 20		90 ± 20	
final	-6.4 ± 17.2	60	10 ± 7	2	66 ± 27	4	94 ± 27	4
24 Pleito								
prior	-0.2 ± 20.0		10 ± 5		65 ± 20		90 ± 20	
final	-10.8 ± 15.8	66	9 ± 7	4	67 ± 18	56	96 ± 21	41
25 Garlock W								
prior	.0 ± 10.0		10 ± 5		65 ± 20		90 ± 20	
final	21.8 ± 7.0	73	13 ± 5	46	50 ± 11	84	84 ± 18	55
26 Garlock E								
prior	-3.0 ± 20.0		10 ± 5		90 ± 10		180 ± 10	
final	7.0 ± 9.4	88	11 ± 7	2	91 ± 13	1	179 ± 13	1
27 Garlock E								
prior	-3.0 ± 20.0		10 ± 5		90 ± 10		180 ± 10	
final	-4.3 ± 3.6	98	10 ± 6	10	90 ± 13	2	182 ± 13	8

Table 3.

Derived Fault Parameters

Fault/ model	Block Slip (mm/yr)	Block Convergence (mm/yr)	Strike Slip (mm/yr)	Dip Slip (mm/yr)	Creep Rate (mm/yr)
Ozena					
prior	2.4 ± 28.3	1.3 ± 28.3	3.0 ± 20.0	0.0 ± 0.5	-0.6 ± 34.6
final	2.2 ± 5.2	-1.1 ± 3.8	3.0 ± 7.1	-0.1 ± 0.7	-0.8 ± 10.5
Big Pine W					
prior	6.3 ± 28.3	1.4 ± 28.3	6.0 ± 20.0	0.0 ± 1.0	0.3 ± 34.6
final	-4.5 ± 4.6	1.7 ± 3.7	-6.2 ± 5.1	+0.1 ± 1.4	1.7 ± 8.0
Big Pine C					
prior	5.0 ± 28.3	4.0 ± 28.3	6.0 ± 20.0	0.0 ± 3.1	-1.0 ± 34.6
final	1.5 ± 5.2	1.8 ± 4.1	2.1 ± 9.6	0.0 ± 1.5	-0.6 ± 11.7
Big Pine E					
prior	4.5 ± 28.3	7.4 ± 28.3	9.0 ± 20.0	0.0 ± 3.1	-4.5 ± 34.6
final	3.3 ± 5.5	3.3 ± 2.9	5.0 ± 7.7	0.0 ± 2.3	-1.6 ± 11.1
Pine Mtn W					
prior	.0 ± 28.3	0.0 ± 28.3	0.0 ± 10.0	0.0 ± 0.0	0.0 ± 30.0
final	-6.4 ± 5.5	2.1 ± 3.8	-8.2 ± 6.6	-1.8 ± 5.7	1.9 ± 10.1
Sta Ynez W					
prior	.0 ± 28.3	0.0 ± 28.3	0.0 ± 10.0	0.0 ± 0.0	0.0 ± 30.0
final	-2.2 ± 4.4	1.8 ± 3.4	3.7 ± 10.5	+0.3 ± 2.7	-5.9 ± 12.5
Sta Ynez E					
prior	.0 ± 28.3	0.0 ± 28.3	0.0 ± 10.0	0.0 ± 0.0	0.0 ± 30.0
final	-2.6 ± 4.6	0.9 ± 3.1	-4.3 ± 5.3	-0.9 ± 3.2	1.7 ± 8.4
Pine Mtn E					
prior	.0 ± 28.3	0.0 ± 28.3	0.0 ± 10.0	0.0 ± 0.0	0.0 ± 30.0
final	-9.2 ± 5.0	0.4 ± 3.2	-1.9 ± 10.8	0.0 ± 1.4	-7.3 ± 12.5
San Cayetano					
prior	7.1 ± 28.3	10.8 ± 28.3	0.0 ± 0.0	0.0 ± 20.0	7.1 ± 28.3
final	0.1 ± 2.7	2.4 ± 2.1	-4.3 ± 4.0	-10.6 ± 8.4	4.4 ± 4.6
Sta Susana W					
prior	9.7 ± 28.3	8.5 ± 28.3	0.0 ± 0.0	0.0 ± 20.0	9.7 ± 28.3
final	0.8 ± 2.7	2.3 ± 2.2	-0.5 ± 1.3	+3.1 ± 4.8	1.3 ± 2.5
Sta Susana E					
prior	3.9 ± 28.3	12.3 ± 28.3	0.0 ± 0.0	0.0 ± 20.0	3.9 ± 28.3
final	-0.6 ± 2.7	2.4 ± 2.1	-6.9 ± 2.2	+4.1 ± 1.8	6.3 ± 3.2
San Gabriel N					
prior	1.2 ± 28.3	5.5 ± 28.3	0.0 ± 0.0	0.0 ± 20.0	1.2 ± 28.3
final	8.5 ± 3.7	-3.7 ± 4.5	7.2 ± 7.2	+16.1 ± 12.0	1.3 ± 7.8
San Gabriel W					
prior	-0.9 ± 28.3	5.5 ± 28.3	0.0 ± 0.0	0.0 ± 20.0	-0.9 ± 28.3
final	3.1 ± 2.8	6.5 ± 2.8	17.8 ± 9.4	-35.8 ± 8.6	-14.7 ± 9.2

Table 3. Derived Fault Parameters

Fault/ model	Block Slip (mm/yr)	Block Convergence (mm/yr)	Strike Slip (mm/yr)	Dip Slip (mm/yr)	Creep Rate (mm/yr)
Sierra Madre					
prior	5.8 ± 28.3	13.7 ± 28.3	0.0 ± 0.0	0.0 ± 20.0	5.8 ± 28.3
final	0.5 ± 2.8	9.5 ± 2.2	4.3 ± 8.1	-30.5 ± 17.7	-3.8 ± 8.2
Cucamonga					
prior	0.0 ± 28.3	14.8 ± 28.3	0.0 ± 0.0	0.0 ± 20.0	0.0 ± 28.3
final	-3.3 ± 2.8	9.0 ± 2.2	-7.4 ± 7.1	-20.6 ± 8.4	4.1 ± 7.7
San Andreas A					
prior	31.0 ± 28.3	-1.1 ± 28.3	31.0 ± 20.0	0.0 ± 5.4	0.0 ± 34.6
final	21.8 ± 6.1	10.6 ± 8.1	23.8 ± 5.4	+0.4 ± 5.1	-1.9 ± 8.5
San Andreas B					
prior	25.2 ± 28.3	2.7 ± 28.3	35.0 ± 20.0	0.0 ± 6.1	-9.8 ± 34.6
final	19.0 ± 6.8	0.6 ± 4.0	17.7 ± 8.3	-0.2 ± 4.1	1.3 ± 12.7
San Andreas C					
prior	33.2 ± 28.3	6.0 ± 28.3	35.0 ± 20.0	0.0 ± 6.1	-1.8 ± 34.6
final	23.6 ± 7.1	1.3 ± 3.7	34.0 ± 13.9	-4.6 ± 7.2	-10.4 ± 17.9
San Andreas D					
prior	36.9 ± 20.0	1.7 ± 20.0	35.0 ± 20.0	0.0 ± 6.1	1.9 ± 28.3
final	16.1 ± 2.6	0.7 ± 1.0	13.0 ± 4.1	+1.3 ± 2.4	3.2 ± 5.6
San Andreas E					
prior	36.9 ± 20.0	-1.8 ± 20.0	35.0 ± 20.0	0.0 ± 6.1	1.9 ± 28.3
final	16.1 ± 2.6	-0.8 ± 1.1	16.4 ± 2.8	+2.7 ± 1.7	-0.2 ± 4.5
San Andreas F					
prior	36.3 ± 20.0	-7.0 ± 20.0	0.0 ± 20.0	0.0 ± 0.0	36.3 ± 28.3
final	15.8 ± 2.5	-3.1 ± 1.3	-25.6 ± 22.3	-0.3 ± 6.1	41.5 ± 22.6
White Wolf W					
prior	-10.8 ± 28.3	11.5 ± 28.3	0.0 ± 0.0	-0.2 ± 20.0	-10.8 ± 28.3
final	-20.6 ± 7.5	10.1 ± 6.9	-0.5 ± 3.2	-6.4 ± 17.1	-20.2 ± 8.6
White Wolf E					
prior	-5.7 ± 28.3	11.4 ± 28.3	0.0 ± 0.0	-0.2 ± 20.0	-5.7 ± 28.3
final	-11.5 ± 6.8	5.8 ± 5.8	-1.2 ± 4.2	-10.1 ± 15.8	-10.4 ± 8.1
Pleito					
prior	-3.4 ± 28.3	3.8 ± 28.3	0.0 ± 0.0	0.0 ± 10.0	-3.4 ± 28.3
final	-2.8 ± 5.5	9.7 ± 3.7	-2.2 ± 6.9	+21.7 ± 7.0	-0.6 ± 7.1
Garlock W					
prior	5.2 ± 20.0	-4.4 ± 20.0	-3.0 ± 20.0	0.0 ± 0.5	8.2 ± 28.3
final	4.3 ± 4.3	-5.2 ± 4.0	6.9 ± 9.4	+0.2 ± 1.6	-2.6 ± 11.3
Garlock E					
prior	-0.1 ± 20.0	-4.5 ± 20.0	-3.0 ± 20.0	0.0 ± 0.5	2.9 ± 28.3
final	-5.0 ± 2.5	-0.7 ± 1.3	-4.3 ± 3.6	+0.1 ± 1.0	-0.6 ± 5.2

FIGURE CAPTIONS

Fig. 1. Fault geometry and notation. The dislocation rate (\dot{D}), the fault width (W), the dip angle (δ), and the slip angle (λ) are all treated as unknown parameters. The depth to the upper fault edge (d) is fixed.

Fig. 2. Map showing faults, both as mapped and as idealized for this study; blocks; and trilateration monuments (triangles). Blocks are named in Table 1, and faults named in Table 2. The area shown is 210 km by 170 km.

Fig. 3. Prior and final estimates of block motion. Final estimates indicate slower displacement across the San Andreas Fault than do the prior estimates.

Fig. 4. Estimated block slip (that is, parallel slip at depth). Shaded arrows indicate right lateral motion, open arrows left lateral.

Fig. 5. Estimated block convergence. Arrows pointing towards faults indicate convergence, arrows pointing away indicate divergence.

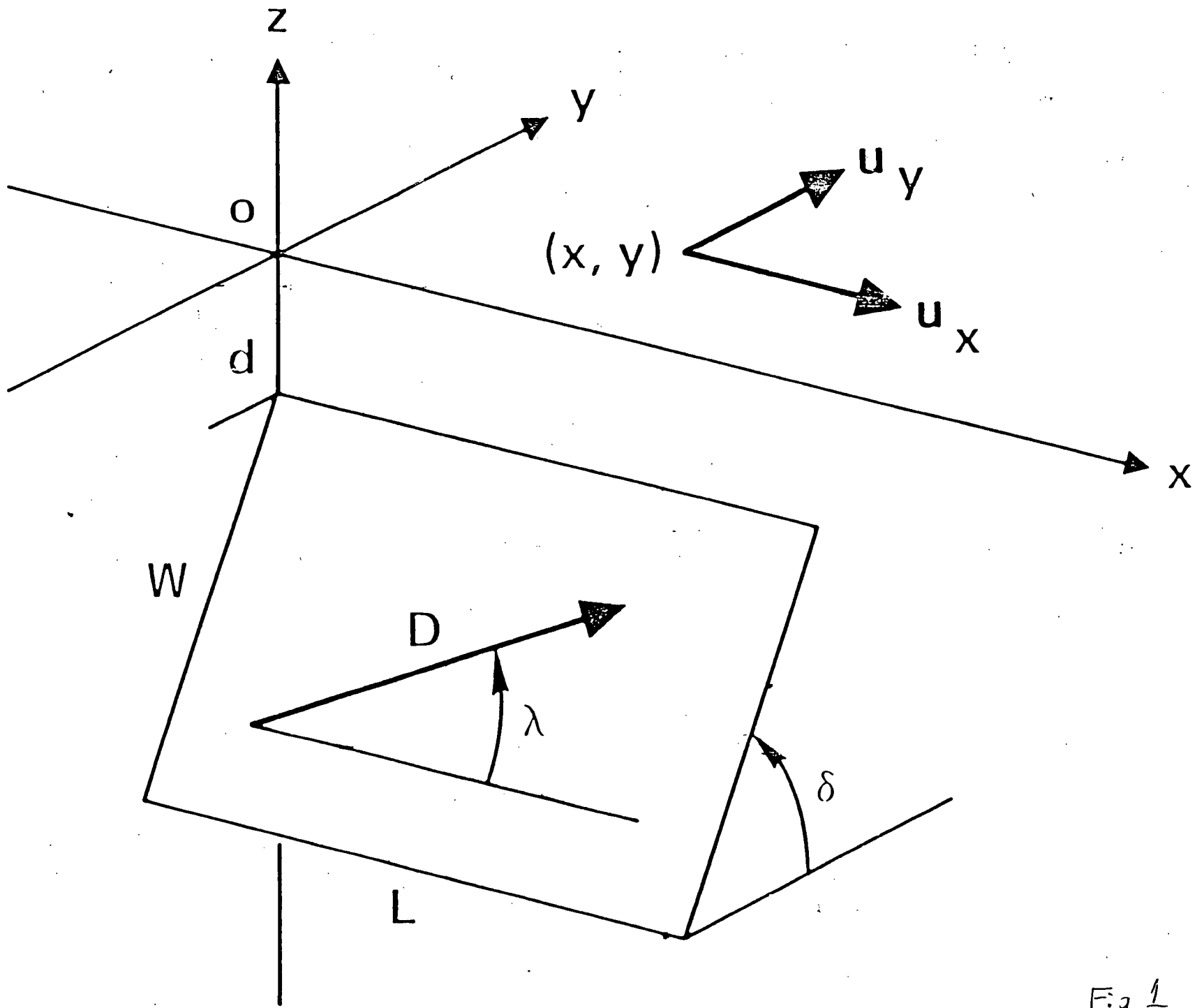


Fig 1

TRANSVERSE RANGES

(Fault and Block Notation)

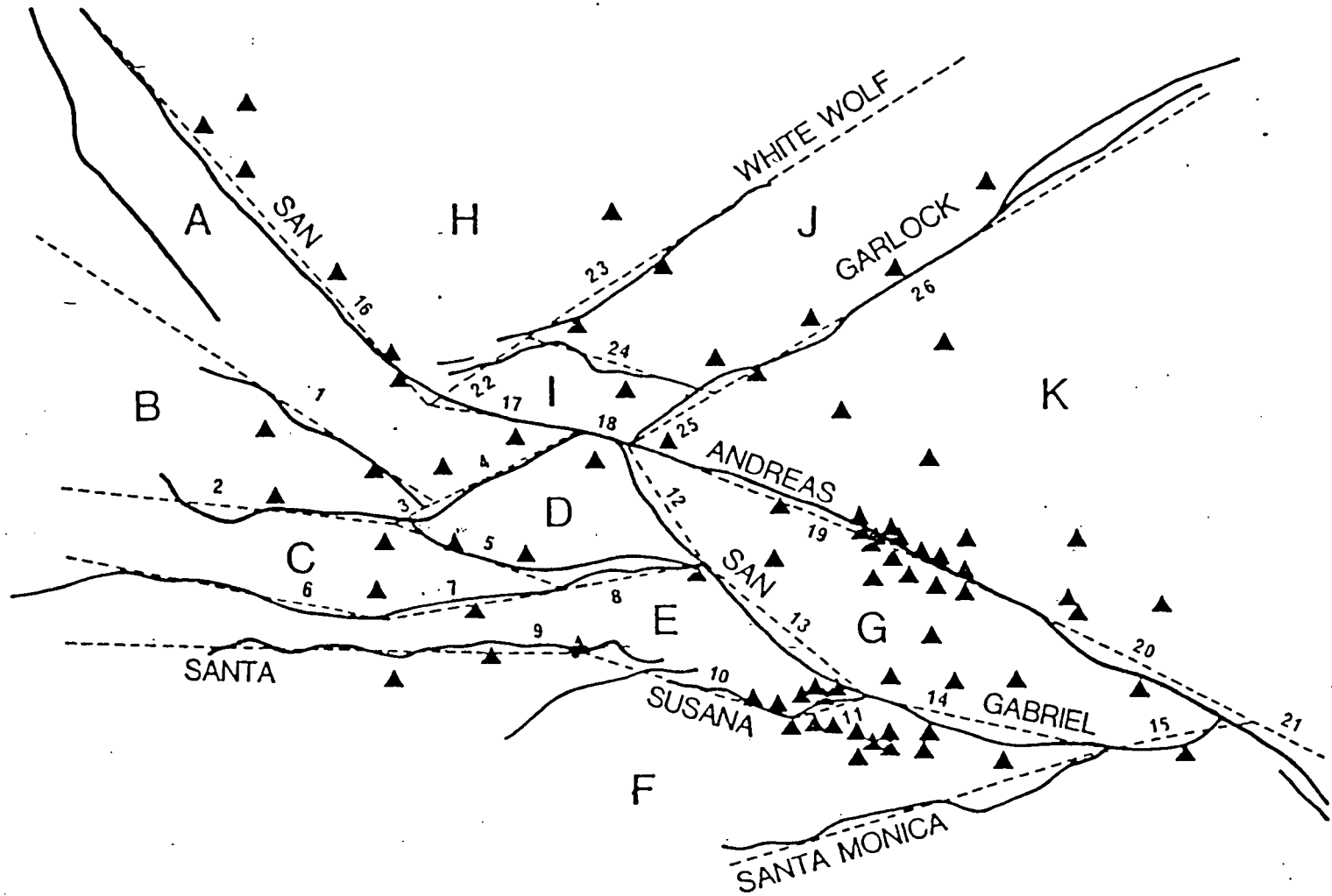


Fig 2

TRANSVERSE RANGES

(Block Motion: initial and final)

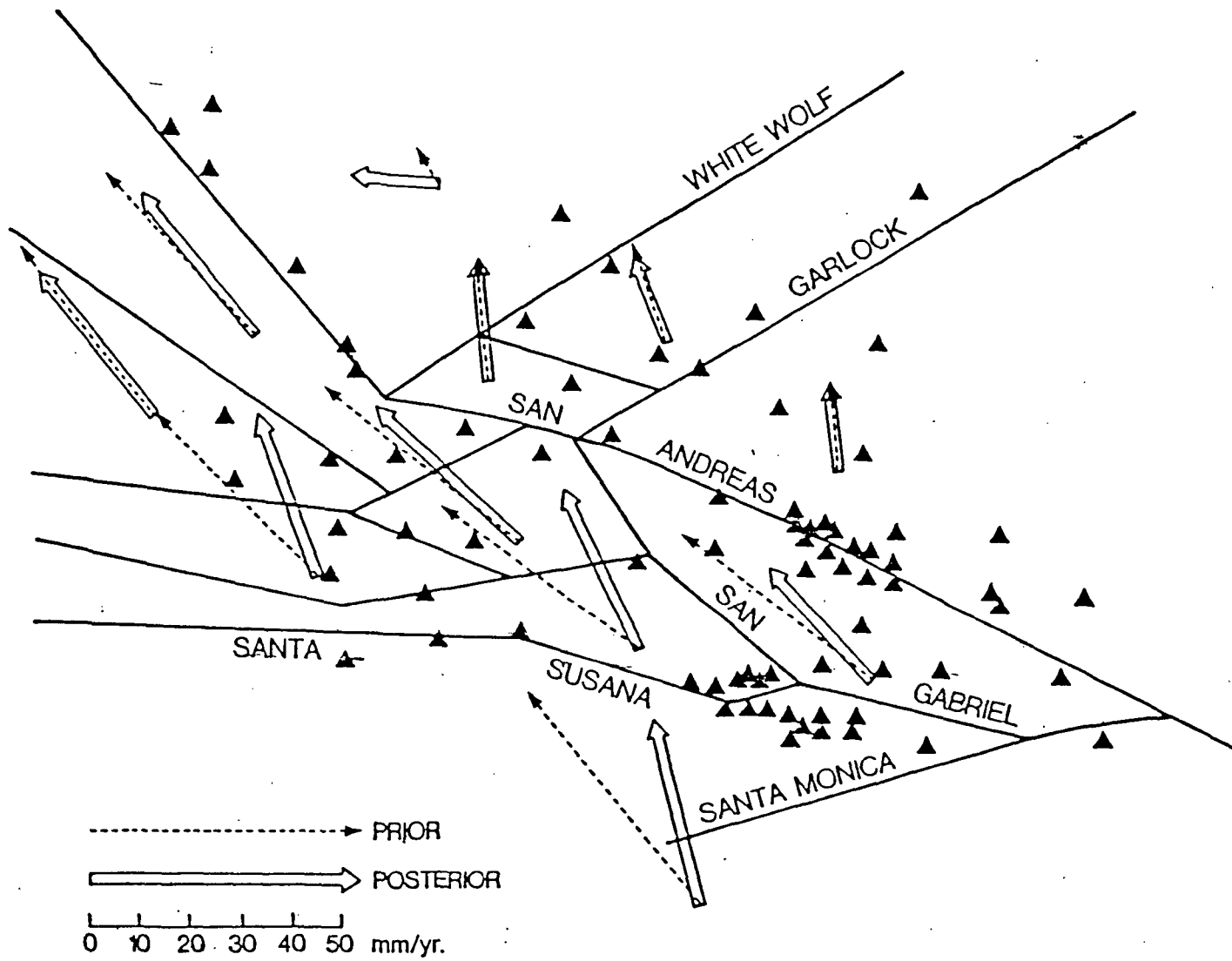


Fig 3

TRANSVERSE RANGES

(Fault Slip)
Block

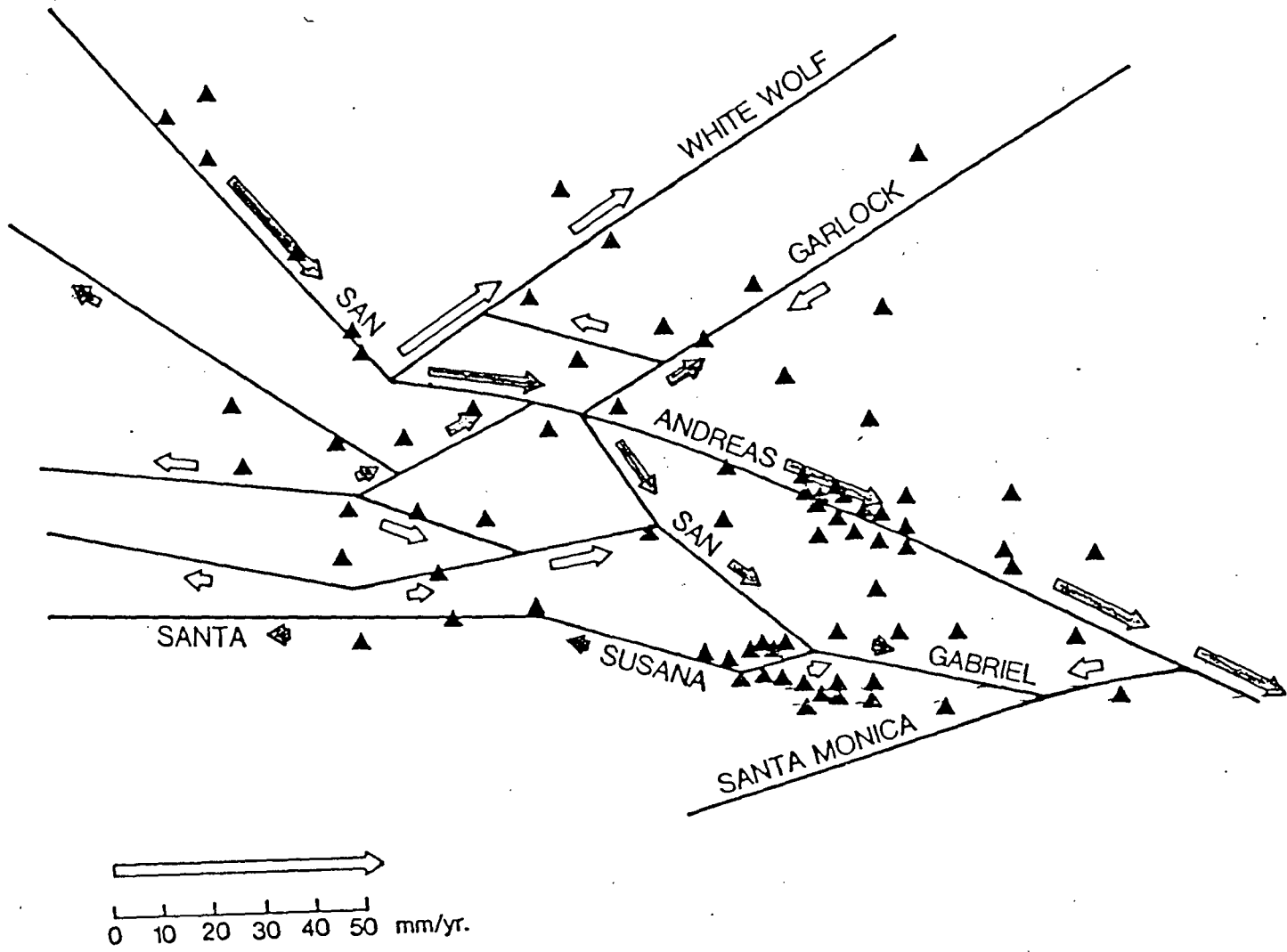


Fig 4

TRANSVERSE RANGES (Block Convergence)

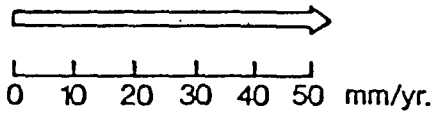
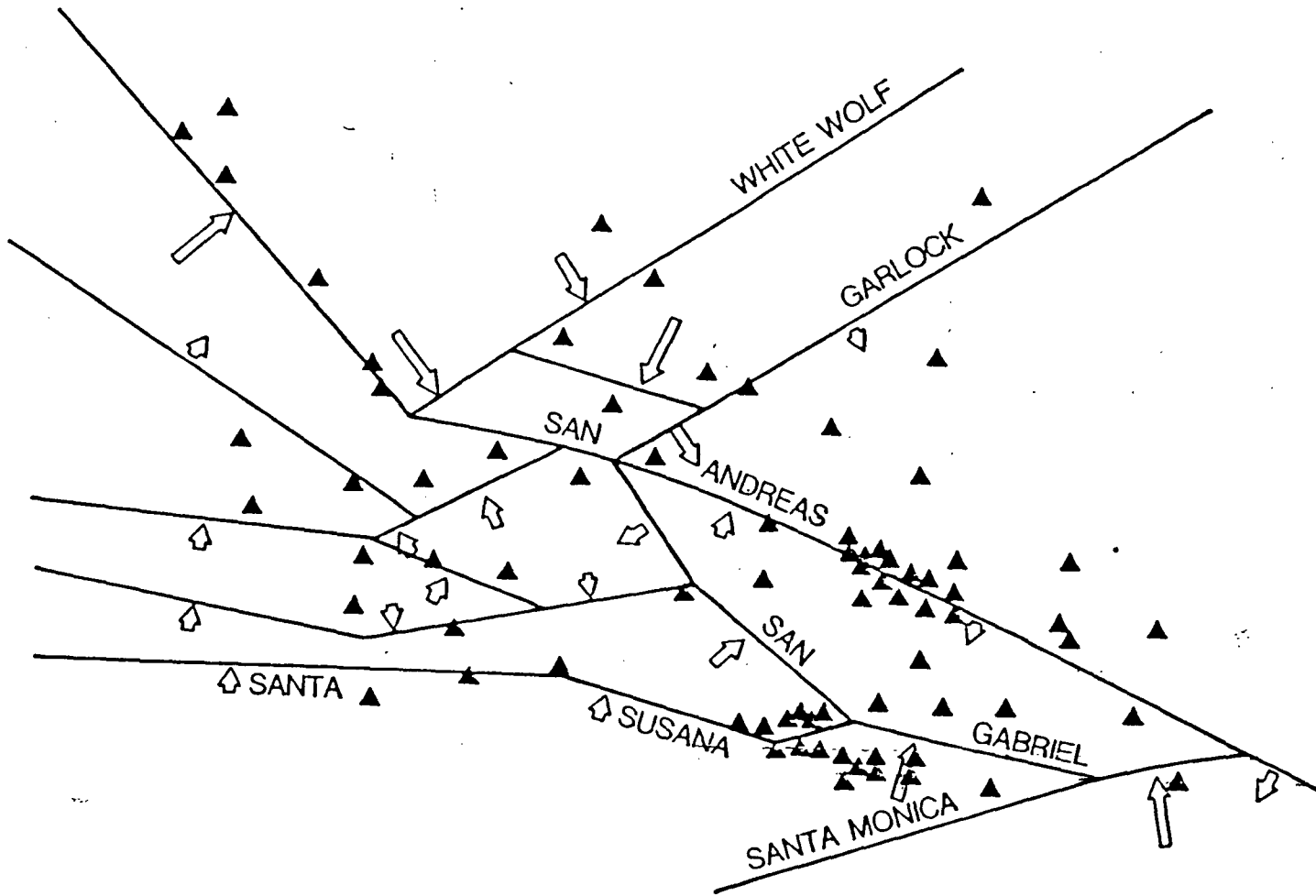


Fig 5.